3D-Printed Microfluidic Sensor in SIW Technology for Liquids Characterization

Giulia Maria Rocco, *Student Member*, *IEEE*, Maurizio Bozzi, *Fellow*, *IEEE*, Dominique Schreurs, *Fellow*, *IEEE*, Luca Perregrini, *Fellow*, *IEEE*, Stefania Marconi, Gianluca Alaimo, and Ferdinando Auricchio

***Abstract*—This paper presents the implementation of a novel microfluidic sensor based on a resonant cavity. The cavity is based on the substrate integrated waveguide (SIW) technology and is fabricated by using stereolithographic 3D printing, which guarantees fast prototyping and allows arbitrary geometry. The proposed sensor consists of a square cavity and an inner meander pipe provided with two openings, where the liquid under test is injected and extracted, and is fed by a coaxial probe, which represents the microwave port of the circuit. S-parameter measurement allows retrieving the electromagnetic properties of the liquid injected in the pipe. In particular, the loss tangent of the liquid is extracted from the variation of the cavity quality factor compared to air-filled pipe, after removing the actual losses of the structure. The dielectric permittivity of the liquid is retrieved from the shift of the cavity resonance frequency relative to the case of air-filled pipe, without any hypothesis of small losses. The performance of the sensor is discussed through the electromagnetic characterization of several fluids.**

***Index Terms*—Additive manufacturing, 3D printing, microfluidic sensor, permittivity measurement, substrate integrated waveguide (SIW) technology.**

I. INTRODUCTION

ADDITIVE manufacturing technology is drawing a lot of interest in science and engineering fields [1]. Nowadays, commercial 3D printers merge low cost and high accuracy, and a large number of degrees of freedom are available to the final user. The most interesting feature of 3D-printing technology is the suitability to realize devices with complex shapes [2]-[4], not feasible by classical milling machines, based on subtractive technologies. Moreover, the availability of flexible materials is exploited to realize strain and wearable sensors [5]-[7]. Thanks to these features, 3D printing technology has been widely used, in the last years, to develop microwave devices for the new generation of wireless sensors networks [8], expected for Internet of Things applications [9]. Among the proposed devices, great importance is given to biomedical "smart health" applications [10].

Towards the development of devices for real-time health monitoring, a lot of attention has been drawn by microfluidics-based microwave sensors. They are designed and fabricated for handling small quantities of liquids for numerous chemical and biological applications [11]-[14]. These sensors can be small, inexpensive, and permit to detect and characterize materials in an accurate way.

Microfluidic sensors are well known in the microwave literature: they are commonly realized as coplanar waveguide resonator [15], interdigitated capacitor [16], split ring resonator, or complementary split ring resonator [17]-[19]. Generally, these solutions are implemented by commercial (low-loss) laminates, arranged in a stratified fashion, with Polydimethylsiloxane (PDMS) or SU-8 layers for the microfluidic channel.

The novelty of the microfluidic sensor proposed in this work consists in the use of a 3D printed cavity resonator that embeds a multi-folded pipe. The main advantage of the proposed solution is the complete flexibility in the design of the pipe and the cavity. Moreover, the whole structure of the sensor consists of a single dielectric substrate, realized in a one-pass, low-cost, and rapid fabrication process. The sensor is implemented by adopting the substrate integrated waveguide (SIW) technology [20]-[21], which enables the implementation of low–loss and cost-effective structures, from components and antennas to complete systems. The use of SIW technology in the implementation of the microfluidic sensor offers a simple yet effective solution for the metallization of the structure, which can be achieved by using top and bottom aluminum or copper tape [4], and screws or metal rivets for the side posts [22].

The other significant contribution of this work is the rigorous approach used to retrieve the dielectric permittivity and the loss tangent of the liquids under test: the loss tangent is obtained from the quality factor, after deembedding the losses of the sensor, whereas the dielectric permittivity is derived from the resonance frequency shift, taking into account also the loss tangent of the liquid.

The preliminary idea of this sensor and the geometry of the microfluidic cavity was introduced in [23]. The present paper significantly extends the theoretical work, discussing a more accurate technique to retrieve the electrical characteristics of

Submitted 16 May 2019; revised 22 October 2019; accepted 29 Oct. 2019.

G.M. Rocco, M. Bozzi and L. Perregrini are with the Department of Electrical, Computer, and Biomedical Engineering, University of Pavia, 27100 Pavia, Italy (e-mail: giuliamaria.rocco01@universitadipavia.it, maurizio.bozzi@unipv.it, luca.perregrini@unipv.it).

D. Schreurs is with the TELEMIC Division of Department of Electrical Engineering (ESAT), University of Leuven, Leuven 3001, Belgium (e-mail: dominique.schreurs@kuleuven.be).

G. Alaimo, S. Marconi, and F. Auricchio are with the Department of Civil Engineering and Architecture, University of Pavia, 27100 Pavia, Italy (e-mail: gianluca.alaimo01@universitadipavia.it; stefania.marconi@unipv.it; auricchi@unipv.it).

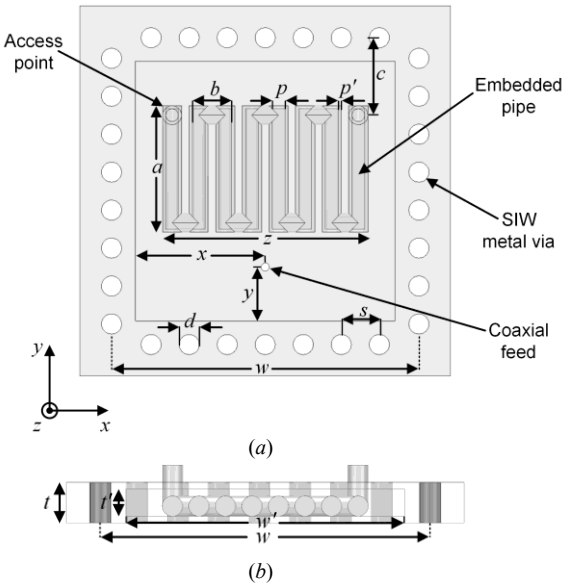

Fig. 1. Geometry of the proposed 3D-printed microfluidic sensor: (a) top view (dimensions in mm: a=20.12, b=5.51, c=12.25, d=3.2, p=1.6, p'=0.76, s=6, w=48.5, x=20.5, y=9, z=30.42); (b) side view (dimensions in mm: w=48.5, w'=41, t=6, t'=4).

the liquids, and it applies the sensor to the characterization of a wide number of liquids. In particular, de-ionized water/isopropanol mixtures were used, with isopropanol volume fraction ranging from 0% to 100%. Moreover, a rigorous comparison with measurements performed by a commercial coaxial probe is presented and discussed through the use of error bar diagrams.

The paper is organized as follows. Section II presents the design procedure and the fabrication of the microfluidic sensor by 3D printing. Section III reports the experimental characterization of the sensor, to determine the resonance frequency and the quality factor, when the micro-pipe is filled with different liquids. Section IV discusses the novel techniques developed to retrieve the dielectric permittivity and the loss tangent of the liquids from the measured data. Finally, Section V discusses the accuracy of the method through error bars, and Conclusions are drawn in Section VI.

II. DESIGN AND FABRICATION OF THE SENSOR

The structure of the proposed sensor consists of a square SIW cavity with an embedded multi-folded pipe, where the liquid can be injected and extracted, respectively, through two vertical access points (Fig. 1). This cavity operates with the fundamental TM_{110} mode (with respect to the z axis), whose resonance frequency is related to both the cavity's transversal dimensions and the effective dielectric permittivity of the material filling the cavity. When a liquid is injected into the pipe, the effective permittivity inside the cavity changes, thus causing a variation of the resonance frequency and of the quality factor of the cavity mode. In particular, replacing the air inside the pipe with a liquid (liquid under test, LUT), the effective permittivity increases and, consequently, the resonance frequency decreases. In addition, the losses associated with the liquid are higher than losses of air, thus causing a reduction of the quality factor of the cavity mode. In practical applications, the variation of the resonance frequency allows to retrieve the relative permittivity of the LUT, whereas the variation of the quality factor permits to determine the losses of the LUT (although the two relations are not rigorously independent).

In this work, a 3D printer has been adopted for the fabrication of the entire structure, including the cavity and the multi-folded pipe. The use of 3D printing allows large flexibility in the design of both the cavity and the pipe shape and size. A drawback of using 3D-printed materials are the pretty large dielectric losses associated with these materials, which leads to a small quality factor of the (empty) cavity resonator. In the specific case, large losses in the cavity resonator could jeopardize the accurate retrieval of the loss tangent of the LUT. To mitigate this issue and to keep the quality factor as high as possible, the dielectric filling of the cavity was minimized in the design. Instead of realizing a cavity completely filled of 3D-printed dielectric material, the cavity consists of an external dielectric shell. In the design of the pipe, the walls have the minimum thickness that avoids leakage of the liquid. The pipe was located near the bottom of the cavity for easier fabrication.

A. Design of the microfluidic sensor

The resonant cavity of the sensor is connected to the exterior through a coaxial probe, located in a side portion of the cavity. The location of the coaxial probe has been selected far enough from the pipe, and optimized to have the best coupling condition for the fundamental cavity mode. As shown in Fig. 5, the return loss, in all simulations with LUTs, is larger than 10 dB. This guarantees pronounced peaks in the $|S_{11}|$ parameter and, in turn, it allowed to extract the resonance frequencies in a more accurate way.

The sensor has been designed to operate in the lower portion of the ultra-wide band (UWB), in the frequency range from 3.4 GHz to 3.8 GHz. This is an important point, if we consider a future implementation with other blocks within the wireless sensor network panorama [24]-[25].

The choice of the length a of the pipe, as well as the number of turns, is the result of a trade-off: if the length of the pipe is too short, the frequency shift of the cavity mode when injecting the liquid is limited, thus resulting in small sensitivity in the determination of the dielectric permittivity of the LUT. If the length of the pipe is too long, the losses of the liquid reduce significantly the quality factor of the cavity mode, thus leading to a poor retrival of the dielectric characteristics of the LUT.

Finally, a dielectric layer with thickness 1 mm was located at the top and the bottom of the cavity, to provide two planes suitable for metallization in the fabrication phase. To realize the side walls of the cavity, holes in the dielectric material were printed, in order to accommodate metal screws.

B. Characterization of the 3D printed material

Before determining the optimized dimensions of the microfluidic sensor, the precise knowledge of the dielectric characteristics of the 3D-printed material are needed.

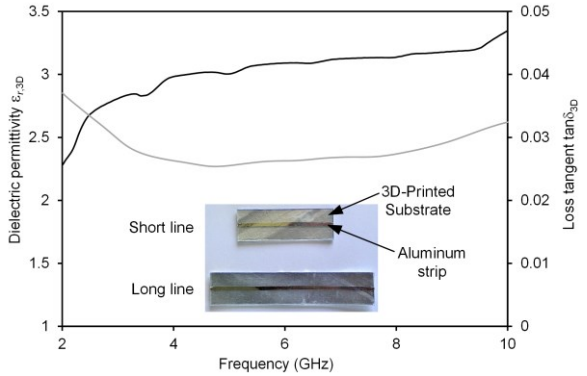

Fig. 2. Broadband measurements of the dielectric characteristics of the 3D-printed material (Clear FLGPCL02).

The printable material selected for the implementation of the microfluidic sensor was Clear FLGPCL02, a photopolymeric resin used by Formlabs stereolithographic (SLA) printers. Clear FLGPCL02 was chosen because it permits to realize watertight walls for the micro-pipe where the fluid is injected, and because it is transparent, thus allowing to control the integrity of the pipe once the sensor is printed.

The 3D-printed material has been characterized in the frequency range of interest, and the dielectric permittivity $\varepsilon_{r,3D}$ and the loss tangent $\tan\delta_{3D}$ have been retrieved by using a microstrip line approach [26],[27]. Two samples with equal thickness of 1 mm and different lengths have been 3D printed and then two microstrip lines have been fabricated by using aluminum tape pasted on substrate faces to realize the ground plane and the microstrip line. The retrieved values are shown in Fig. 2. The 3D-printed material exhibits a rather constant behavior, and the values of $\varepsilon_{r,3D} = 2.9$ and $\tan\delta_{3D} = 0.03$ have been adopted in the design.

Based on the results of the electromagnetic characterization of the 3D-printed material, the final dimensions of the sensor have been optimized by adopting the commercial electromagnetic solver Ansys HFSS. The dimensions of the sensor are reported in the caption of Fig. 1.

C. Fabrication of the microfluidic sensor

The fabrication of the sensor substrate has been performed by using a FormLabs Form2 SLA printer. This process consists in having a vat of liquid photopolymer resin, out of which the model is built layer-by-layer by photo-polymerization. An ultraviolet light determines the link of chains of molecules, thus forming polymers. While the light cures or hardens the resin, the printer platform moves the object. For the manufacturing of the sensor, 20 ml of resin has been used, with a spacial resolution of 50 µm. A photograph of the 3D-printed structure is shown in Fig. 3(*a*).

Once the photopolymeric portion of the sensor has been printed, the metallization was applied in two steps: firstly, the top and bottom layers were covered with adhesive aluminum tape; subsequently, stainless steel screws were used to define the side walls of the SIW cavity. The distance *s* between these screws was set to fit them in the cavity boundary, also taking into account the recommended spacing needed to avoid radiation leakage, which is twice the screw diameter [28].

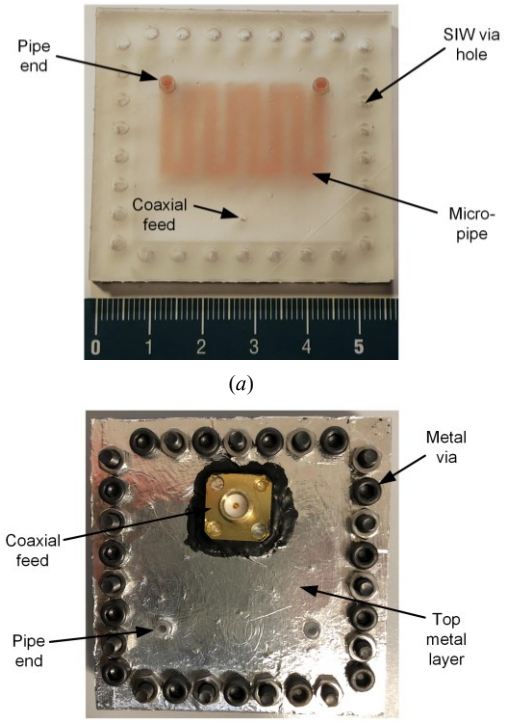

(*a*)

(*b*)

Fig. 3. Prototype of the microfluidic sensor: (*a*) Photograph with colored water to highlight the embedded micro-pipe; (*b*) Photograph of the sensor after metallization.

Finally, the pin of an SMA connector was inserted in the small hole created during the 3D-printing phase, with the aim to feed the cavity. Moreover, a conductive paint from Bare Conductive was used to guarantee the electrical contact between the connector and the metal tape. A photograph of the sensor after metallization is reported in Fig. 3(*b*).

III. MEASUREMENTS

A. Measurement setups

Two measurement setups have been prepared (Fig. 4) for the determination of the electrical characteristics of the LUT.

In the first setup, the proposed microfluidic sensor is connected with a flexible cable to a PXIe VNA Keysight M9375A, which performs S-parameter measurements. The measurement frequency was swept from 2 GHz to 5 GHz, and the VNA output power was set to -20 dBm, to prevent any microwave heating. A pressure pump by Fluigent was used to inject the LUT inside the pipe of the sensor with a constant pressure. Using the software interface by MAESFLO, it was possible to adjust the pressure of the pump and stop the injection as soon as the pipe is full. This measurement setup is shown in Fig. 4(*a*).

The second one is based on the commercial open-ended coaxial probe Keysight N1501A Dielectric Probe Kit, operating over the frequency range from 0.5 GHz to 50 GHz, and which is used as the reference method. As shown in Fig. 4(*b*), the open-ended coaxial probe is connected through a flexible coaxial cable to the vector network analyzer (VNA) Keysight E8361A. Proprietary software converts the measured reflection coefficient into the complex dielectric permittivity of the LUT.

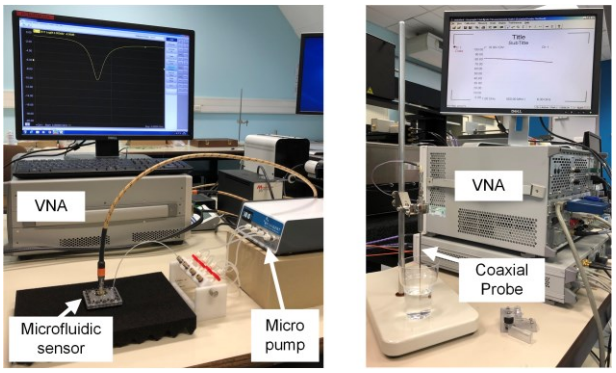

(*a*) (*b*)

Fig. 4. Measurement setups: (*a*) S-parameter measurements of the sensor; (*b*) Commercial coaxial probe for the liquids characterization.

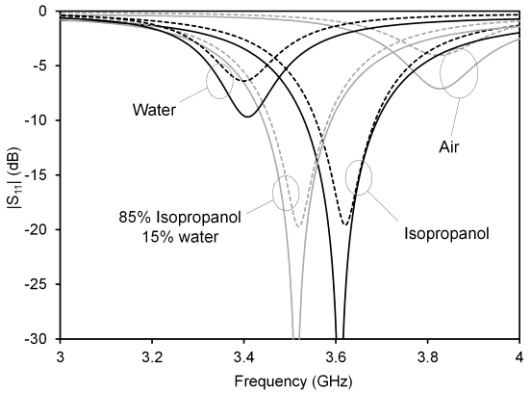

Fig. 5. Simulated (solid lines) and measured (dashed lines) reflection coefficient $|S_{11}|$ for air, pure isopropanol, mixture of 85% isopropanol and 15% water, and distilled water.

B. Results

By using the first measurement setup, the scattering parameter $|S_{11}|$ at the coaxial port of the microfluidic sensor was measured when filling the pipe with different LUTs. Fig. 5 shows the measured $|S_{11}|$ for four different cases (air, isopropanol 100%, a mixture of 85% isopropanol and 15% water, and distilled water). As expected, the resonance frequency of the cavity decreases when moving from air-filled, or empty, to water-filled pipe, i.e., when increasing the dielectric permittivity of the LUT. More specifically, the resonance frequencies change from 3.826 GHz with the empty pipe to 3.408 GHz with the water-filled pipe. In addition to the frequency shift, the quality factor of the cavity changes when modifying the liquid in the pipe.

The resonance frequency f_0 and the unloaded quality factor Q_U^{meas} of the cavity can be derived from the measured S-parameters. The resonance frequency is obtained as the frequency corresponding to the minimum of $|S_{11}|$. The unloaded quality factor is calculated along the lines of [29], [30]. Starting from the measured reflection coefficient $|S_{11}|$, the half-power width is calculated as $f_2 - f_1$, where f_1 and f_2 are the frequencies where

$$|S_{11}| = \sqrt{\frac{\left|S_{11}^{b}\right|^2 + \left|S_{11}^{min}\right|^2}{2}} \tag{1}$$

where $\left|S_{11}^{b}\right|$ is the base-line value of $|S_{11}|$ out of resonance, and $\left|S_{11}^{min}\right|$ is the value of $|S_{11}|$ at the resonance frequency. The loaded quality factor Q_L^{meas} is determined as the ratio between the resonance frequency f_0 and the half-power bandwidth $f_2 - f_1$

$$Q_L^{meas} = \frac{f_0}{f_2 - f_1}. \tag{2}$$

To derive Q_U^{meas}, the coupling coefficient k has to be determined from the linear value of $\left|S_{11}^{min}\right|$ as

$$k = \frac{1-\left|S_{11}^{min}\right|}{1+\left|S_{11}^{min}\right|} \quad \text{or} \quad k = \frac{1+\left|S_{11}^{min}\right|}{1-\left|S_{11}^{min}\right|} \tag{3}$$

for the undercoupling and overcoupling cases, respectively. From Q_L^{meas} and k, the unloaded quality factor Q_U^{meas} of the resonator can be calculated as

$$Q_U^{meas} = Q_L^{meas}(1+k). \tag{4}$$

The values of f_0 and Q_U^{meas} retrieved from measured data are reported in Table I, for air, distilled water, isopropanol, and seven different mixtures of water and isopropanol.

By using the second measurement setup, the dielectric characteristics of different liquids have been measured over the entire frequency range of interest. The dielectric permittivity and the loss tangent of all LUTs, each measured at the resonance frequency obtained in previous case, are reported in Table II.

TABLE I
VALUES OF MEASURED RESONANCE FREQUENCY, FREQUENCY SHIFT AND UNLOADED QUALITY FACTOR WHEN THE PIPE IS FILLED WITH LIQUIDS

Mixture Under Test	Resonance frequency f_0 (GHz)	Frequency shift Δf (GHz)	Unloaded quality factor Q_U^{meas}
Air	3.8267	0	43.12
Water 100%	3.4077	0.4190	36.73
Isoprop. 10%/Water 90%	3.4150	0.4117	34.24
Isoprop. 20%/Water 80%	3.4174	0.4093	31.78
Isoprop. 30%/Water 70%	3.4243	0.4024	29.06
Isoprop. 45%/Water 55%	3.4287	0.3980	27.31
Isoprop. 60%/Water 40%	3.4474	0.3793	24.03
Isoprop. 75%/Water 25%	3.4757	0.3510	21.47
Isoprop. 85%/Water 15%	3.5147	0.3120	18.12
Isopropanol 100%	3.6095	0.2172	17.48

TABLE II
REFERENCE VALUES OF DIELECTRIC PERMITTIVITY AND LOSS TANGENT MEASURED BY A COAXIAL PROBE

Mixture Under Test	ε_r	$\tan\delta$
Water 100%	75.6	0.17
Isoprop. 10%/Water 90%	64.9	0.24
Isoprop. 20%/Water 80%	59.2	0.36
Isoprop. 30%/Water 70%	49.9	0.45
Isoprop. 45%/Water 55%	35.3	0.57
Isoprop. 60%/Water 40%	24.9	0.67
Isoprop. 75%/Water 25%	14.8	0.78
Isoprop. 85%/Water 15%	8.04	0.81
Isopropanol 100%	3.90	0.55

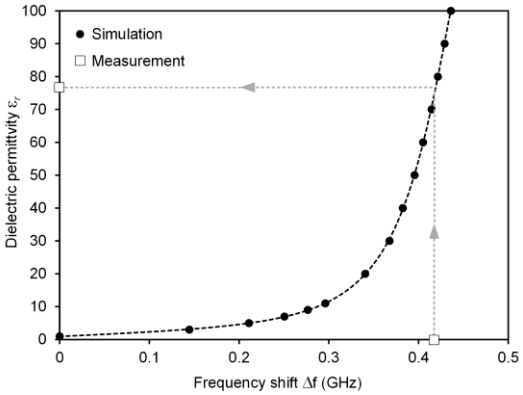

Fig. 6. Simulated values of the dielectric permittivity versus the resonance frequency shift, and experimental validation example for water.

IV. RETRIEVAL OF LUT DIELECTRIC PROPERTIES

The dielectric permittivity of the LUT can be retrieved from the shift of the resonance frequency. To this aim, HFSS simulations have been performed, considering the pipe filled with materials with different dielectric permittivity (ε_r ranging from 1 to 100) and null loss tangent, to calculate the corresponding frequency shift Δf. These analyses led to the simulation curve shown in Fig. 6.

The simulation results were fitted with a rational function, relating the dielectric permittivity ε_r of the LUT to the frequency shift Δf and whose expression is

$$\varepsilon_r = \frac{p_1 \Delta f^3 + p_2 \Delta f^2 + p_3 \Delta f + p_4}{\Delta f^2 + q_1 \Delta f + q_2} \tag{5}$$

where p_1=14.96, p_2=-8.889, p_3=1.826, p_4=0.2086, q_1=-0.924, and q_2 = 0.2183. This particular fitting function was chosen because this shape allows to get a very low RMSE < 0.4 and R^2 = 0.999. In this way, the plot in Fig. 6 or the expression in (5) allow to retrieve the dielectric permittivity of the LUT from the measured frequency shift.

The example of water is shown in Fig. 6. When water is injected in the pipe, the measured frequency shift (with respect to the case with empty pipe) was Δf=0.419 GHz. According to (5) or the plot in Fig. 6, the corresponding permittivity of water resulted in ε_r = 76.6 (square marker in Fig. 6). This approach was applied to all LUTs considered in this work. The resulting values of dielectric permittivity were then used in the following section.

A. Loss Tangent Retrieval – Proposed Method

In order to retrieve the loss tangent tanδ of the LUT, the variation of the unloaded quality factor is exploited. This section presents a method to retrieve the correct loss tangent of the LUT, independently of potential inaccuracies in the determination of the value of the characteristics of the 3D printed material, and in particular its loss tangent $\tan\delta_{3D}$.

In the simulations, the unloaded quality factor of the cavity Q_U^{sim} depends on the losses in the 3D printed structure and on the conductors (characterized by Q_{3D+C}^{sim}) and on the losses in the liquid in the pipe (characterized by Q_{liq}^{sim}), according to the relation

$$\frac{1}{Q_U^{sim}} = \frac{1}{Q_{liq}^{sim}} + \frac{1}{Q_{3D+C}^{sim}} \tag{6}$$

Based on (6), the value of the quality factor Q_{liq}^{sim}, due to losses in the liquid, can be expressed as

$$\frac{1}{Q_{liq}^{sim}} = \frac{1}{Q_U^{sim}} - \frac{1}{Q_{3D+C}^{sim}} \tag{7}$$

where Q_U^{sim} is the quality factor obtained from the simulation of the entire sensor (including the lossy liquid in the pipe), while Q_{3D+C}^{sim} is related both to the 3D-printed structure and to the conductors losses , and it is obtained from the simulation of the sensor with lossless liquid in the pipe (so that losses depend on the 3D-printed material and conductors only).

Assuming that the main source of error is the poor estimation of the losses due to the 3D-printed structure, a different strategy to estimate Q_{3D}^{sim} is needed. A reasonable estimate of the losses in the 3D-printed structure can be obtained from the measurements. In fact, the quality factor Q_{3D+C}^{meas} can be reasonably estimated by the measured quality factor $Q_{U,air}^{meas}$ of the structure with empty pipe. Therefore, in (6)

$$Q_{3D}^{sim} \rightarrow Q_{3D+C}^{meas} = Q_{U,air}^{meas}. \tag{8}$$

It is noted that the accuracy of this approach is limited by the fact that the field distribution in the cavity is slightly different with or without the presence of the liquid in the pipe.

By substituting (7) and (8) in (6), a modified expression for the quality factor extracted from a combination of simulations and measurements is obtained, which is defined by $Q_U^{sim,ref}$

$$\frac{1}{Q_U^{sim,ref}} = \frac{1}{Q_U^{sim}} - \frac{1}{Q_{3D+C}^{sim}} + \frac{1}{Q_{U,air}^{meas}} \tag{9}$$

where the first term of the right-hand side takes into account the losses in the LUT, and the second and third term represent the refinement of the losses in the 3D-printed structure, obtained by replacing the simulated value with the measured one.

This transformation is shown in the plot reported in Fig. 7. By using the values of permittivity extracted according to the method described at the beginning of this section, HFSS simulations were performed for each material, with the retrieved value of ε_r and the loss tangent varying from 0 to 1. The results of these simulations are represented by the black markers, which can be fitted by a rational function

$$\tan\delta = \frac{p_1 Q_U^{sim\,3} + p_2 Q_U^{sim\,2} + p_3 Q_U^{sim} + p_4}{Q_U^{sim\,2} + q_1 Q_U^{sim} + q_2} \tag{10}$$

where p_1=-0.002965, p_2=0.04461, p_3=17.92, p_4=1.533, q_1=-12.49, and q_2=0.4673. The fitting function is represented by the black dashed curve, and relates the loss tangent to the quality factor Q_U^{sim}. If the refined estimation of the losses in the metallized 3D-printed structure ($Q_{U,air}^{meas}$) is taken into account, the white markers are obtained, which represent $Q_U^{sim,ref}$. The fitting function used to interpolate the samples of $Q_U^{sim,ref}$ has the

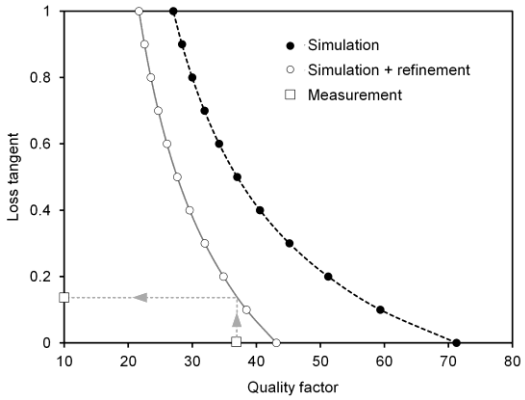

Fig. 7. Simulated values of the loss tangent versus the unloaded quality factor, with the traditional method (Q_U^{sim}) and the proposed method ($Q_U^{sim,ref}$), along with the experimental validation example for water (Q_U^{meas}).

same expression of (10) apart from the coefficients, which in this case are p_1=-0.01036, p_2=0.2325, p_3=9.03, p_4=1.609, q_1 =-12.42, and q_2=-0.448.

In Fig. 7, the example of water is reported: in this case, the simulated value of the quality factor related to losses of the metallized 3D-printed structure is Q_{3D+C}^{sim}=71.26, whereas the measured quality factor of the structure filled with air is $Q_{U,air}^{meas}$=43.12 (Table I).

By using the unloaded quality factor Q_U^{meas} obtained from the measured S-parameters, the loss tangent tanδ of the LUT can be retrieved by using Fig. 7. Since the unloaded quality factor of water was Q_U^{meas}=36.7, the resulting loss tangent was tanδ=0.150 (square marker), reasonably close to the reference value obtained with the coaxial probe (tanδ=0.174).

The same technique was applied to all LUTs considered in this work, and the results are reported in Table III. The error in the determination of the loss tangent is in all the cases less than or at least equal to 12%.

B. Dielectric Permittivity Retrieval – Proposed Method

The method for retrieving the dielectric permittivity described at the beginning of section IV does not provide accurate results. In fact, that approach is based on the assumption that the resonance frequency of a cavity resonator depends on the real part of the dielectric permittivity, as the imaginary part (which involves the loss tangent) can be neglected when losses are small.

The general formula for the complex resonance frequency f_c in a resonant cavity can be expressed as [31]

$$f_c = \frac{k_0}{2\pi\sqrt{\varepsilon\,\mu}} \tag{11}$$

where k_0 is the wave number in vacuum and ε and μ are the complex values of permittivity and permeability, respectively.

In the case of lossless, non-magnetic dielectric materials, the permittivity becomes $\varepsilon = \varepsilon_0\varepsilon_r$ and the permeability becomes $\mu = \mu_0$. Consequently, expression (11) can be reformulated as

$$f_c = \frac{k_0}{2\pi\sqrt{\varepsilon_0\varepsilon_r\,\mu_0}} = \frac{k_0\,c}{2\pi\sqrt{\varepsilon_r}} \tag{12}$$

where $c=1/\sqrt{\varepsilon_0\,\mu_0}$ is the speed of light in vacuum.

Conversely, in the case of materials with dielectric losses, the permittivity is expressed as $\varepsilon = \varepsilon_0\varepsilon_r(1 - j\tan\delta)$, and (11) can be expressed as

$$f_c = \frac{k_0\,c}{2\pi\sqrt{\varepsilon_r(1 - j\tan\delta)}}. \tag{13}$$

thus showing how the resonance frequency also depends on the loss tangent of the material in the cavity.

In the simple method used to retrieve the dielectric permittivity of the material, the frequency shift was completely attributed to the dielectric permittivity ε_r, being the simulations performed with tan δ=0. A more accurate retrieval of the permittivity can be obtained by accounting for the effect of losses.

By considering that the resonant frequency f_0=Re$[f_c]$ and comparing (12) and (13), a correction factor can be derived for the value of dielectric permittivity retrieved by the simple method, where the frequency shift was attributed to the permittivity value only. From (12) and (13) it results

$$\frac{1}{\sqrt{\varepsilon_r}} \rightarrow \mathrm{Re}\left[\frac{1}{\sqrt{\varepsilon_r(1 - j\tan\delta)}}\right] \tag{14}$$

By algebraic manipulation of (14), the correction factor is obtained

$$\varepsilon_r \rightarrow \frac{\varepsilon_r}{2}\cdot\frac{\sqrt{1+\tan\delta^2}+1}{1+\tan\delta^2}. \tag{15}$$

Table IV reports the values of ε_r obtained from (15), compared with the nominal values obtained through the coaxial probe characterization method.

Table V presents a comparison between the performance of the proposed sensor and the state-of-art sensors proposed in the literature. The advantage of the proposed microfluidic sensor, with respect to the other devices, is the fact that it allows to characterize liquids with a wide range of permittivity and with a good sensitivity. Moreover, it has to be noticed that, while the other sensors were realized on standard low loss substrate, the proposed sensor has been completely fabricated through 3D-printing.

TABLE III
LOSS TANGENT RETRIEVED WITH THE PROPOSED METHOD AND REFERENCE VALUES MEASURED WITH THE COAXIAL PROBE

Mixture Under Test	Microfluidic Sensor	Coaxial Probe	% Relative error
Water 100%	0.150	0.174	-13.9
Isoprop. 10%/Water 90%	0.238	0.242	-1.61
Isoprop. 20%/Water 80%	0.331	0.356	-6.93
Isoprop. 30%/Water 70%	0.478	0.451	+6.09
Isoprop. 45%/Water 55%	0.594	0.574	+3.49
Isoprop. 60%/Water 40%	0.755	0.675	+11.86
Isoprop. 75%/Water 25%	0.776	0.775	+0.12
Isoprop. 85%/Water 15%	0.910	0.815	+12.03
Isopropanol 100%	0.597	0.554	+7.79

TABLE IV
DIELECTRIC PERMITTIVITY RETRIEVED WITH THE PROPOSED METHOD AND REFERENCE VALUES MEASURED WITH THE COAXIAL PROBE

Mixture Under Test	Microfluidic Sensor	Coaxial Probe	% Relative error
Water 100%	75.3	75.6	-0.4
Isoprop. 10%/Water 90%	64.7	64.9	-0.4
Isoprop. 20%/Water 80%	59.7	59.2	+0.9
Isoprop. 30%/Water 70%	48.9	49.9	-2.1
Isoprop. 45%/Water 55%	42.0	35.3	+19
Isoprop. 60%/Water 40%	26.9	24.9	+8.3
Isoprop. 75%/Water 25%	16.5	14.8	+11.6
Isoprop. 85%/Water 15%	8.60	8.04	+7.5
Isopropanol 100%	4.20	3.90	+7.1

TABLE V
COMPARISON OF THE PROPOSED SENSOR WITH THE STATE OF THE ART

Sensor	f_{air} (GHz)	Frequency shift (GHz)	ε_r range	Meas. Sensitivity $S=\frac{f_{air}-f_{\varepsilon_r}}{f_{air}(\varepsilon_r-1)}\cdot 100$	Ref.
Planar resonator & PDMS pipe	22.6	4.7	20-40	0.53	[32]
CSSR & glass pipe	2.37	0.065	9-79	0.03	[33]
CSSR & PDMS pipe	2	0.48	9-79	0.30	[34]
CSSR & PDMS channel	2	0.7	30-80	0.44	[35]
3D-printed cavity & pipe	3.82	0.42	4-76	0.15	This paper

V. ERROR BARS AND DISCUSSION

The assessment of the accuracy of the proposed method is performed through the analysis of measurement error bars. Fig. 8 reports the values of dielectric permittivity and loss tangent retrieved from measurements, compared with the reference values obtained by using the coaxial probe, for the different liquids considered in this work. For both methods, the plots show the corresponding measurement error bars. The

black error bars are relative to the coaxial probe results, while the grey ones correspond to the values retrieved by using the microfluidic sensor.

The black error bars have been generated considering the typical accuracy of the coaxial probe, reported in the datasheet. For the Keysight Slim Form Probe, the error is given in terms of the uncertainty in the real and imaginary parts of the dielectric permittivity. The uncertainty in ε_r and $\tan\delta$ is then extracted:

$$\Delta\varepsilon_r = \pm 0.1\varepsilon_r\,|1 - j\tan\delta| \tag{16}$$

$$\Delta\tan\delta = \pm 0.1\tan\delta\,|1 - j\tan\delta|\sqrt{\left(1+\frac{1}{\tan\delta}\right)^2} \tag{17}$$

In particular, in the case of $\tan\delta$, the uncertainty is computed by using the error propagation formula [36].

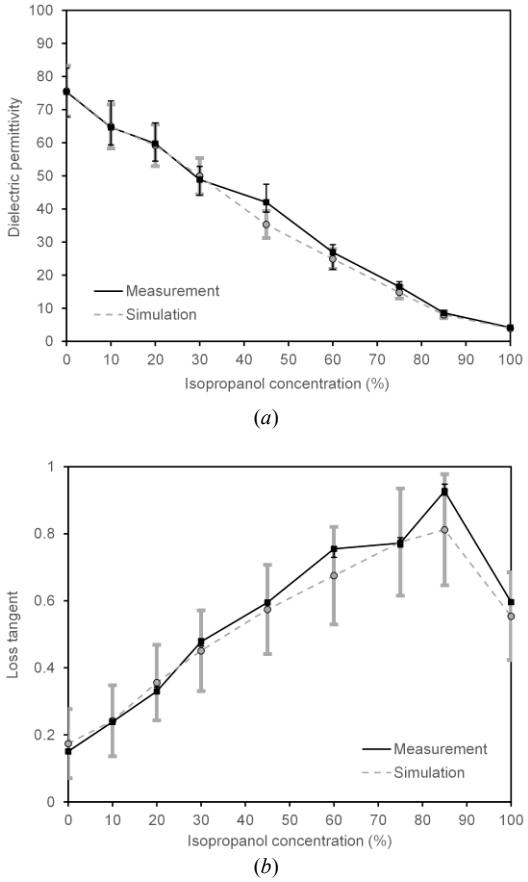

Fig. 8. Comparison between the retrieved and reference values of the dielectric characteristics, with error bars: (*a*) Dielectric permittivity; (*b*) Loss tangent.

In order to generate the error bars corresponding to the values extracted from the S-parameter measurements, we used the datasheet of the PXIe Vector Network Analyzer, which reports the uncertainty of the reflection coefficient with 85052D standard mechanical 3.5 mm calibration kit. In the frequency range of interest (2-4 GHz), the uncertainty in the magnitude of the reflection coefficient $|S_{11}|$ is equal to ± 0.0041. This potential error has an effect on the value of $|S_{11}|$ at resonance and, consequently, on the measured quality factor and resonance frequency. A variation of $|S_{11}^{\min}|$ determines a change in the half-power bandwidth and in the coupling factor *k*, and, therefore, in the unloaded quality factor. On the other hand, if $|S_{11}^{\min}|$ changes, the value of the resonance frequency can be different, either higher or lower, which implies a change in the frequency shift, thus giving rise to an inaccuracy in the calculation of the dielectric permittivity.

In the computation of dielectric permittivity inaccuracy, it was not mentioned the contribution of the VNA step size in the measurements. This is because it can be completely neglected: in the VNA measurement setup, the step size was set equal to 0.94 MHz, which thus gives a maximum percentage error in the calculation of ε_r which is less than 2%.

As shown Fig. 8, the uncertainty in the values of dielectric permittivity and loss tangent retrieved with the proposed method are considerably lower than the uncertainty of the probe, especially in the case of loss tangent measurements.

VI. CONCLUSION

This paper presents a novel kind of microfluidic sensor, which combines the benefits of 3D-printing with the advantages of SIW technology. The structure of the proposed sensor consists in a one-port SIW cavity with an embedded micro-pipe, where the fluid can be injected and extracted, with the aim to determine its electromagnetic properties. A novel method was developed to retrieve the dielectric permittivity and the loss tangent of the liquid from the measured scattering parameter $|S_{11}|$. The main feature of this method is the deembedding of the losses of the 3D-printed structure, which represent the largest source of error. Several measurements have been performed, and mixtures with different concentration of isopropanol have been used in order to test the efficiency of the proposed method over a wide range of values of dielectric permittivity and loss tangent.

REFERENCES

[1] E. MacDonald *et al.*, "3D Printing for the Rapid Prototyping of Structural Electronics," *IEEE Access*, vol. 2, no. 1, pp. 234-242, Dec. 2014.

[2] R. Bahr, B. Tehrani, and M. M. Tentzeris, "Exploring 3-D Printing for New Applications: Novel Inkjet- and 3-D-Printed Millimeter-Wave Components, Interconnects, and Systems," *IEEE Microwave Magazine*, vol. 19, no. 1, pp. 57-66, Jan.-Feb. 2018.

[3] J.G. Hester *et al*., "Additively Manufactured Nanotechnology and Origami-Enabled Flexible Microwave Electronics," *Proceedings of the IEEE*, vol. 103, no. 4, pp. 583-606, April 2015.

[4] S. Moscato *et al*., "Additive manufacturing of 3D substrate integrated waveguide components," *Electronics Letters*, vol. 51, no. 18, pp. 1426-1428, Sept. 2015.

[5] S. A. Nauroze *et al*., "Additively Manufactured RF Components and Modules: Toward Empowering the Birth of Cost-Efficient Dense and Ubiquitous IoT Implementations," *Proceedings of the IEEE*, vol. 105, no. 4, pp. 702-722, April 2017.

[6] M. Rizwan, M. W. A. Khan, L. Sydänheimo, J. Virkki, and L. Ukkonen, "Flexible and Stretchable Brush-Painted Wearable Antenna on a Three-Dimensional (3-D) Printed Substrate," *IEEE Antennas and Wireless Propagation Letters*, vol. 16, pp. 3108-3112, 2017.

[7] R. Colella and L. Catarinucci, "Wearable UHF RFID Sensor-Tag Based on Customized 3D-Printed Antenna Substrates," *IEEE Sensors Journal*, vol. 18, no. 21, pp. 8789-8795, 1 Nov.1, 2018.

[8] S.-H. Yang, *Wireless Sensor Networks: Principles Design and Applications*, Springer, 2014.

[9] D. Giusto, A. Iera, G. Morabito, and L. Atzori (Eds.), *The Internet of Things*, Springer, 2010.

[10] L. Catarinucci *et al*., "An IoT-Aware Architecture for Smart Healthcare Systems," *IEEE Internet of Things Journal*, vol. 2, no. 6, pp. 515-526, Dec. 2015.

[11] K. Grenier *et al*., "Integrated Broadband Microwave and Microfluidic Sensor Dedicated to Bioengineering," *IEEE Transactions on Microwave Theory and Techniques*, vol. 57, no. 12, pp. 3246-3253, Dec. 2009.

[12] D. P. Rose *et al.*, "Adhesive RFID Sensor Patch for Monitoring of Sweat Electrolytes," *IEEE Transactions on Biomedical Engineering*, vol. 62, no. 6, pp. 1457-1465, June 2015.

[13] Chou *et al*., "Fabrication and Characteristic Analysis for Enzymatic Glucose Biosensor Modified by Graphene Oxide and Magnetic Beads Based on Microfluidic Framework," *IEEE Sensors Journal*, vol. 17, no. 6, pp. 1741-1748, 15 March15, 2017.

[14] N. Meyne, G. Fuge, H. K. Trieu, A. Zeng, and A. F. Jacob, "Miniaturized Transmission-Line Sensor for Broadband Dielectric Characterization of Biological Liquids and Cell Suspensions," *IEEE Transactions on Microwave Theory and Techniques*, vol. 63, no. 10, pp. 3026-3033, Oct. 2015.

[15] T. Chretiennot, D. Dubuc, and K. Grenier, "A Microwave and Microfluidic Planar Resonator for Efficient and Accurate Complex Permittivity Characterization of Aqueous Solutions," *IEEE Transactions on Microwave Theory and Techniques*, vol. 61, no. 2, pp. 972-978, Feb. 2013.

[16] X. Bao *et al*., "Broadband Dielectric Spectroscopy of Cell Cultures," *IEEE Transactions on Microwave Theory and Techniques*, vol. 66, no. 12, pp. 5750-5759, Dec. 2018.

[17] D. J. Rowe, S. al-Malki, A. A. Abduljabar, A. Porch, D. A. Barrow, and C. J. Allender, "Improved Split-Ring Resonator for Microfluidic Sensing," *IEEE Transactions on Microwave Theory and Techniques*, vol. 62, no. 3, pp. 689-699, March 2014.

[18] P. Vélez, L. Su, K. Grenier, J. Mata-Contreras, D. Dubuc, and F. Martín, "Microwave Microfluidic Sensor Based on a Microstrip Splitter/Combiner Configuration and Split Ring Resonators (SRRs) for Dielectric Characterization of Liquids," *IEEE Sensors Journal*, vol. 17, no. 20, pp. 6589-6598, 15 Oct.15, 2017

[19] A. Ebrahimi, W. Withayachumnankul, S. Al-Sarawi, and D. Abbott, "High-Sensitivity Metamaterial-Inspired Sensor for Microfluidic Dielectric Characterization," *IEEE Sensors Journal*, vol. 14, no. 5, pp. 1345-1351, May 2014.

[20] D. Deslandes and K. Wu, "Integrated microstrip and rectangular waveguide in planar form," *IEEE Microwave and Wireless Components Letters*, Vol. 11, No. 2, pp. 68-70, Feb. 2001.

[21] M. Bozzi, A. Georgiadis, and K. Wu, "Review of Substrate Integrated Waveguide (SIW) circuits and antennas," *IET Microwaves, Antennas and Propagation*, Vol. 5, No. 8, pp. 909–920, June 2011.

[22] R. Moro, S. Agneessens, H. Rogier, A. Dierck, and M. Bozzi, "Textile Microwave Components in Substrate Integrated Waveguide Technology," IEEE Transactions on Microwave Theory and Techniques, Vol. 63, No. 2, pp. 422-432, February 2015.

[23] G.M.Rocco, M. Bozzi, S. Marconi, G. Alaimo, F. Auricchio, and D. Schreurs, "3D-Printed Microfluidic Sensor in Substrate Integrated Waveguide Technology," *IEEE MTT-S International Microwave Workshop Series-Advanced Materials and Processes* (IMWS-AMP 2018), Ann Arbor, USA, 16-18 July 2018.

[24] J. Zhang, P. V. Orlik, Z. Sahinoglu, A. F. Molisch, and P. Kinney, "UWB Systems for Wireless Sensor Networks," in *Proceedings of the IEEE*, vol. 97, no. 2, pp. 313-331, Feb. 2009.

[25] A. Costanzo, D. Masotti, M. Fantuzzi, and M. Del Prete, "Co-Design Strategies for Energy-Efficient UWB and UHF Wireless Systems," *IEEE Transactions on Microwave Theory and Techniques*, vol. 65, no. 5, pp. 1852-1863, May 2017.

[26] E. Massoni, L. Silvestri, G. Alaimo, S. Marconi, M. Bozzi, L. Perregrini, and F. Auricchio, "3D-Printed Substrate Integrated Slab Waveguide for Single-Mode Bandwidth Enhancement," *IEEE Microwave and Wireless Components Letters*, vol. 27, no. 6, pp. 536-538, June 2017.

[27] D. M. Pozar, *Microwave Engineering,* John Wiley & Sons, 2005.

[28] R. Garg, I. Bahl, and M. Bozzi, *Microstrip Lines and Slotlines*, Third Edition, Artech House, May 2013.

[29] L. F. Chen, C. K. Ong, C. P. Neo, V. V. Varadan, and V. K. Varadan, *Microwave Electronics: Measurement and Materials Characterization*, Hoboken, NJ, USA: Wiley, 2004.

[30] R. J. Cameron, C. M. Kudsia, and R. Mansour, *Microwave Filters for Communication Systems*, John Wiley & Sons, 2007.

[31] K. Kurokawa, *An Introduction to the Theory of Microwave Circuits*, Academic Press, 1969.

[32] T. Chretiennot, D. Dubuc and K. Grenier, "A Microwave and Microfluidic Planar Resonator for Efficient and Accurate Complex Permittivity Characterization of Aqueous Solutions," *IEEE Transactions on Microwave Theory and Techniques,* vol. 61, no. 2, pp. 972-978, Feb. 2013.

[33] E. L. Chuma, Y. Iano, G. Fontgalland, and L. L. Bravo Roger, "Microwave Sensor for Liquid Dielectric Characterization Based on Metamaterial Complementary Split Ring Resonator," *IEEE Sensors Journal*, vol. 18, no. 24, pp. 9978-9983, 15 Dec. 2018.

[34] Ebrahimi, W. Withayachumnankul, S. Al-Sarawi, and D. Abbott, "High-Sensitivity Metamaterial-Inspired Sensor for Microfluidic Dielectric Characterization," *IEEE Sensors Journal*, vol. 14, no. 5, pp. 1345-1351, May 2014.

[35] A. Ebrahimi, J. Scott, and K. Ghorbani, "Ultrahigh-Sensitivity Microwave Sensor for Microfluidic Complex Permittivity Measurement," *IEEE Transactions on Microwave Theory and Techniques*, vol. 67, no. 10, pp. 4269-4277, Oct. 2019.

[36] I. G. Hughes and T. P. A. Hase, *Measurements and their Uncertainties: A practical guide to modern error analysis,* Oxford University Press Inc., New York, NY, USA, 2010.

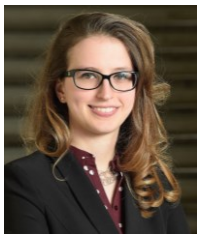

Giulia Maria Rocco (S'15) was born in Pavia, Italy, in 1992. She received the B.S. degree (cum laude) in electronics and computer science and the M.S. degree (cum laude) in electronic engineering from the University of Pavia, Pavia, Italy, in 2014 and 2016, respectively. She is currently pursuing the dual Ph.D. degree in electronics at the University of Pavia and the KU Leuven, Leuven, Belgium. Her research interests include the design of microwave sensors with additive manufacturing techniques.

Ms. Rocco was a recipient of an Undergraduate Scholarship from the IEEE MTT Society in 2016.

Maurizio Bozzi (S'98–M'01–SM'12–F'18) was born in Voghera, Italy, in 1971. He received the Ph.D. degree in electronics and computer science from the University of Pavia, Pavia, Italy, in 2000.

He held research positions with various universities worldwide, including the Technische Universität Darmstadt, Germany; the Universitat de Valencia, Spain; and the École Polytechnique de Montréal, Canada. In 2002, he joined the Department of Electronics, University of Pavia, where he is currently a Full Professor of electromagnetic fields. He was also a Guest Professor at Tianjin University, China (2015-2017) and a Visiting Professor at Gdansk University of Technology, Poland (2017-2018).

He has authored or co-authored more than 130 journal papers and 300 conference papers. He co-edited the book Periodic Structures (Research Signpost, 2006) and co-authored the book Microstrip Lines and Slotlines (Artech House, 2013). His main research interests concern the computational electromagnetics, the substrate integrated waveguide technology, and the use of novel materials and fabrication technologies for microwave circuits (including paper, textile, and 3D printing).

Prof. Bozzi is an Elected Member of the Administrative Committee of the IEEE Microwave Theory and Techniques Society (MTT-S) for terms 2017–2019 and 2020–2022, and the Chair of the Meeting and Symposia Committee of MTT-S AdCom for years 2018–2019. He was the Secretary of IEEE MTT-S for year 2016 and a member of the General Assembly (GA) of the European Microwave Association (EuMA) from 2014 to 2016. He is a track editor of the IEEE TRANSACTIONS ON MICROWAVE THEORY AND TECHNIQUES. He was an associate editor of the IEEE MICROWAVE AND WIRELESS COMPONENTS LETTERS, *IET Electronics Letters*, and *IET Microwaves, Antennas and Propagation*. He was the Guest Editor of special issues in the IEEE TRANSACTIONS ON MICROWAVE THEORY AND TECHNIQUES, the IEEE MICROWAVE MAGAZINE, and the *IET Microwaves, Antennas and Propagation*. He was the General Chair of the IEEE MTT-S International Microwave Workshop Series-Advanced Materials and Processes (IMWS-AMP 2017), in Pavia, Italy, 2017, of the inaugural edition of the IEEE International Conference on Numerical Electromagnetic Modeling and Optimization (NEMO2014), in Pavia, Italy, 2014, and of the IEEE MTT-S International Microwave Workshop Series on Millimeter Wave Integration Technologies, in Sitges, Spain, 2011.

He received several awards, including the 2015 Premium Award for Best Paper in IET Microwaves, Antennas & Propagation, the 2014 Premium Award for the Best Paper in Electronics Letters, the Best Student Paper Award at the 2016 IEEE Topical Conference on Wireless Sensors and Sensor Networks (WiSNet2016), the Best Paper Award at the 15th Mediterranean Microwave Symposium (MMS2015), the Best Student Award at the 4th European Conference on Antennas and Propagation (EuCAP 2010), the Best Young Scientist Paper Award of the XXVII General Assembly of URSI in 2002, and the MECSA Prize of the Italian Conference on Electromagnetics (XIII RiNEm), in 2000.

Dominique Schreurs (S'90–M'97–SM'02–F'12) received the M.Sc. degree in electronic engineering and the Ph.D. degree from the University of Leuven (KU Leuven), Leuven, Belgium.

She has been a Visiting Scientist with Agilent Technologies, Santa Rosa, CA, USA, ETH Zurich, Zürich, Switzerland, and the National Institute of Standards and Technology, Boulder, CO, USA. She is currently a Full Professor with KU Leuven, where she is also the Chair of the Leuven LICT. Her current research interests include the microwave and millimeter-wave characterization and modeling of transistors, nonlinear circuits, and bioliquids, and system design for wireless communications and biomedical applications.

Dr. Schreurs was an IEEE MTT-S Distinguished Microwave Lecturer. She is also the President of the IEEE Microwave Theory and Techniques Society. She was the General Chair of the 2007, 2012, and 2018 Spring ARFTG Conferences. She is currently the President of the ARFTG Organization. She was the Editor-in-Chief of the IEEE Transactions on Microwave Theory and Techniques.

Luca Perregrini (M'97-SM'12-F'16) was born in Sondrio, Italy, in 1964. He received the Laurea degree in Electronic Engineering and the Ph.D. in Electronics and Computer Science in 1989 and 1993, respectively. In 1992 he joined the Faculty of Engineering of the University of Pavia, he is currently full professor of electromagnetic fields and responsible of the Microwave Laboratory. He has been a visiting professor at the École Polytechnique de Montréal, Québec, Canada in 2001, 2002, 2005, and 2006.

He has been responsible of many research contracts with prominent international research centers and companies. His main research interests have been focused on the development of numerical methods for electromagnetics, and the design of microwave components and antennas. He authored or co-authored more than 90 journal papers and more than 250 conference papers, six book chapters, two textbooks, and co-edited the book Periodic Structures, (Research Signpost, 2006). His current research interests include the development of numerical methods for electromagnetics, and the design of microwave components and antennas.

Prof. Perregrini has been an invited speaker at many conferences, and has delivered invited seminar talks in Universities and research centers worldwide. He was a member of the General Assembly of the European Microwave Association (EuMA) from 2011 to 2013. He is a member of the Technical Committee MTT–15 (Microwave Field Theory) of IEEE Microwave Theory and Technique Society (MTT-S), of the Board of Directors of EuMA. He served as a member of prize committees for several conferences/societies.

He is Fellow of the Institute of Electrical and Electronics Engineers (IEEE). He was the co-recipient of several the best paper awards at international conferences. He is the appointed Technical Program Committee Chair of the International Microwave Workshop Series on Advanced Materials and Processes (IMWS-AMP 2017), Pavia, Italy, in 2017. He was the Technical Program Committee Chair of the IEEE MTT-S International Conference on Numerical Electromagnetic Modeling and Optimization (NEMO2014), Pavia, Italy, in 2014, and of the European Microwave Conference, Rome, Italy, in 2014. He was Associate Editor of the IEEE MICROWAVE AND WIRELESS COMPONENTS LETTERS from 2010 to 2013, of IEEE TRANSACTIONS ON MICROWAVE THEORY AND TECHNIQUES from 2013 to 2016, of the International Journal of Microwave and Wireless Technologies from 2011 to 2016, and of IET Electronic Letters from 2015 to 2016. He was Guest Editor of the IEEE TRANSACTIONS ON MICROWAVE THEORY AND TECHNIQUES in 2015 and of the International Journal of Microwave and Wireless Technologies in 2015. He is currently Editor in Chief of the IEEE TRANSACTIONS ON MICROWAVE THEORY AND TECHNIQUES.

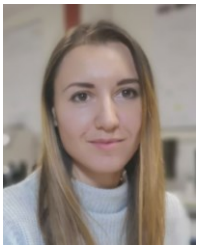

Stefania Marconi received the bachelor and master degree in biomedical engineering from the University of Pavia (Italy), in 2009 and 2011, respectively. She received a Ph.D. in Experimental Surgery and Microsurgery from the Medical Faculty of the University of Pavia, in 2015. She is now a Research Fellow at the Department of Civil Engineering and Architecture of the University of Pavia. Her current research interest is focused on the study of additive manufacturing technologies and materials, with a focus on their application to the medical field, especially for pre-operative simulation and training purposes. She is in charge of supervising the activity of the clinical 3D printing laboratory of IRCCS Policlinico San Matteo in Pavia, Italy. She is a member of the Technological Committee of the European Association of Endoscopic Surgery.

Gianluca Alaimo was born in Palermo, Italy, in 1976. He received the master's degree in mechanical engineering, a Master in Biomechanical engineering and the Ph.D. degree in civil engineering, from the University of Palermo, and Pavia, Italy, in 2012, 2013 and 2018, respectively.

He is currently a Post-Doctoral Fellow at the University of Pavia where is also jointly responsible of the 3D-printing lab. His research interest actually covers additive manufacturing with the related new materials and printing technologies, optimization techniques, numerical simulation of manufacturing processes.

Ferdinando Auricchio received the Bachelor degree in Civil Engineering from the University of Napoli, Italy (1989), and the the Master of Science (1991) and the Ph.D. (1995) from the University of California at Berkeley, USA. Since 2001, he has been a professor of Solids and Structural Mechanics at the University of Pavia, Italy, where he started to develop strong collaborations with the Department of Mathematics (being also a Research Associate at IMATI-CNR Pavia) and with several medical institutions.

He received the Euler Medal by ECCOMAS (European Community of Computational Methods in Applied Sciences) in 2016 and he became Fellow Award by IACM (International Association for Computational Mechanics) since 2012. Since 2013 he is Vice-President of ECCOMAS. In 2018 he was appointed as a member of the Italian National Academy of Science, known also as Accademia dei XL.

Major research interests are the development of numerical schemes (in particular, finite element methods, both for solids and fluids, with a particular attention to innovative materials), the development of simulation tools to support medical decision (in particular, for cardiovascular applications), and more recently everything that is related to additive manufacturing. In fact, he has organized a 3D-printing lab, exploring new materials, new printing technologies, new uses of 3D printing, ranging from civil engineering 3D printed concrete beams to bio-manufacturing.

He has more than 200 publications on refereed international journals, H-index of 43 on Scopus, close to 6000 citations on Scopus.